

RESEARCH PAPER



## SQSTM1-dependent autophagic degradation of PKM2 inhibits the production of mature IL1B/IL-1 $\beta$ and contributes to LIPUS-mediated anti-inflammatory effect

Bin Zhang, Hangang Chen, Junjie Ouyang, Yangli Xie, Liang Chen, Qiaoyan Tan, Xiaolan Du, Nan Su, Zhenhong Ni, and Lin Chen

Center of Bone Metabolism and Repair, State Key Laboratory of Trauma, Burns and Combined Injury, Trauma Center, Research Institute of Surgery, Laboratory for the Prevention and Rehabilitation of Military Training Related Injuries, Daping Hospital, Army medical University (Third Military Medical University), Chongqing, China

### ABSTRACT

Synovitis is implicated in the pathology of osteoarthritis (OA) and significantly contributes to the development of OA. As a noninvasive physical therapy, low-intensity pulsed ultrasound (LIPUS) has been reported to possess anti-inflammatory effect in recent years. However, the role of LIPUS on synovitis of OA and the underlying mechanisms are little known. The present study showed that LIPUS ameliorated synovial inflammation in destabilization of the medial meniscus (DMM) mouse model and air pouch model, and alleviated pain gait patterns of DMM mouse. LIPUS dramatically inhibited the production of mature IL1B/IL-1 $\beta$  (interleukin 1 beta) *in vitro* and *in vivo*. In addition, LIPUS upregulated the macroautophagy/autophagy level as well as accelerated the formation of an SQSTM1 (sequestosome1)-PKM (pyruvate kinase, muscle) complex in the lipopolysaccharide (LPS)-adenosine triphosphate (ATP)-treated macrophages. Besides, LIPUS downregulated the level of PKM2 in LPS-ATP-treated macrophages, which could be reversed by SQSTM1 knockdown. In brief, the present study for the first time demonstrates that LIPUS inhibits the production of mature IL1B partially via SQSTM1-dependent autophagic degradation of PKM2 in LPS-ATP-treated macrophages, which may further ameliorate the synovial inflammation and gait patterns in animal models. Our data provide new clues for the treatments of synovitis and other inflammatory diseases using LIPUS.

**Abbreviations:** 3-MA: 3-methyladenine; ATG7: autophagy-related 7; ATP: adenosine triphosphate; BafA1: bafilomycin A<sub>1</sub>; BMDMs: bone marrow derived macrophages; CHX: cycloheximide; DMM: destabilization of the medial meniscus; ELISA: enzyme-linked immunosorbent assay; GFP: green fluorescent protein; IL1B/IL-1 $\beta$ : interleukin 1 beta; LIPUS: low-intensity pulsed ultrasound; LIR: LC3-interacting region; LPS: lipopolysaccharide; MAP1LC3B/LC3B: microtubule associated protein 1 light chain 3 beta; MDP: muramyl dipeptide; NFKB/NF- $\kappa$ B: nuclear factor kappa B; NLRP3: NLR family, pyrin domain containing 3; OA: osteoarthritis; PKM/PKM2: pyruvate kinase M1/2; PMA: phorbol-12-myristate-13-acetate; PYCARD/ASC; PYD and CARD domain containing; RFP: red fluorescent protein; siRNAs: small interfering RNAs; SQSTM1: sequestosome 1; TEM: transmission electron microscopy

### ARTICLE HISTORY

Received 23 October 2018  
Revised 16 August 2019  
Accepted 3 September 2019

### KEYWORDS



Autophagy; inflammasome; low-intensity pulsed ultrasound; macrophage; PKM/PKM2; SQSTM1; synovitis



### Introduction

Synovitis plays an essential role in the pathogenesis of osteoarthritis (OA) and affects joint function tremendously [1]. Previous studies have demonstrated that more than 89% patients with knee OA suffer from synovitis [2]. In clinic, OA patients with hypertrophy and hyperplasia synovium often suffer from symptoms related to synovitis like morning stiffness, night pain and joint swelling. Hypertrophy and hyperplasia synovium can be assessed by ultrasonography, MRI and arthroscopy in OA patients [3]. Moreover, many inflammatory mediators are detected in synovial fluid and synovial membrane of OA patients [4]. Some strategies that inhibit inflammation dramatically alleviate pathological


phenotypes of experimentally induced OA [5]. Thus, synovitis-targeted therapy is a potential method to alleviate the symptoms and signs of OA patients [3].

The OA patients usually have hyperplastic synovium with an increased number of macrophages [3]. The study using technetium-99m-Etarfolatide (99mTc-EC20) showed that there are numerous activated macrophages in synovium of OA patients, which are strongly associated with knee symptoms [6,7]. Piscoer et al. reported that most of macrophages are activated in murine models of OA, especially at the early stages of disease [8]. Depletion of synovial macrophages ameliorates OA-related phenotype including osteophyte formation and fibrosis in the early stage of murine experimental

**CONTACT** Lin Chen  [Linchen70@163.com](mailto:Linchen70@163.com)  Center of Bone Metabolism and Repair, State Key Laboratory of Trauma, Burns and Combined Injury, Trauma Center, Research Institute of Surgery, Laboratory for the Prevention and Rehabilitation of Military Training Related Injuries, Daping Hospital, Army medical University (Third Military Medical University), Chongqing 400042, China;

Zhenhong Ni  [nizhenhong1986@163.com](mailto:nizhenhong1986@163.com)  Center of Bone Metabolism and Repair, State Key Laboratory of Trauma, Burns and Combined Injury, Trauma Center, Research Institute of Surgery, Laboratory for the Prevention and Rehabilitation of Military Training Related Injuries, Daping Hospital, Army medical University (Third Military Medical University), Chongqing 400042, China

Present affiliation for Bin Zhang is Rehabilitation department, Xingcheng Sanatorium of PLA Strategic Support Force, Xingcheng 125100, China

 Supplemental data for this article can be accessed [here](#).

OA model [9]. In addition, many soluble proinflammatory cytokines and catabolic products are mainly produced by macrophages of synovium, which significantly affect OA progression [4,10]. Recently, Zhang et al. found that M1-polarized macrophages are accumulated in the synovium of OA patients and mice, which promotes the formation of osteophyte and damage of cartilage [11]. Inhibition of macrophages activation in synovium may become a new therapy for OA patients [3,12].

As a noninvasive physical therapy, low-intensity pulsed ultrasound (LIPUS) has been widely used in clinic to promote the healing of fresh bone fracture and non-united fracture [13]. A prospective randomized double-blind placebo-controlled trial showed that LIPUS is a safe physical therapy for relieving pain and improving quality of life of patients with knee OA [14]. Recent studies found that LIPUS presents anti-inflammatory ability in several inflammatory diseases including OA [15], muscle injury [16], traumatic brain injury [17], joint immobilization [18] and chronic prostatitis [19]. Moreover, LIPUS alleviates LPS (lipopolysaccharide)-induced inflammatory responses in osteoblasts through inhibiting the formation of TLR4 (toll like receptor 4)-MYD88 (myeloid differentiation primary response 88) complex and NF $\kappa$ B/NF- $\kappa$ B (nuclear Factor Kappa B) nuclear translocation [20,21]. LIPUS also inhibits the transcriptional level of LPS-induced inflammatory factors in U937 macrophage cells [22]. However, the effects and detailed mechanisms by which LIPUS affects macrophages and synovitis remain to be elucidated.

In this study, we demonstrated for the first time that LIPUS suppressed the production of mature IL1B through enhancing autophagy-mediated degradation of SQSTM1 (sequestosome 1) and the PKM2 isoform of PKM (pyruvate kinase M1/2) in LPS-adenosine triphosphate (ATP)-treated macrophages, which may contribute to the relief of synovial inflammation and improvement of the gait patterns in animal models. Our data provide new insight for LIPUS-based noninvasive treatments of OA synovitis and other inflammatory diseases.

## Results

### **LIPUS ameliorates the pain gait patterns of mouse destabilization of the medial meniscus (DMM) model**

Firstly, we investigated the effects of LIPUS on the gait patterns of mice during the early inflammation phase of a post-traumatic osteoarthritis (PTOA) mice using DMM model. The gait of the injured right hind paw was remarkably changed after DMM surgery (Figure 1A,B and movie S1 for negative mouse, movie S2 for DMM surgery mouse). The DMM surgery mice were then treated with LIPUS (Figure 1C). The parameters of LIPUS were shown in Figure 1D. We traced the change of right hind paw duty cycle, which is a classical parameter representing pain gait (Figure 1E) [23]. As shown in Figure 1F,G, we found that the right hind duty cycle was significantly decreased after DMM surgery in both DMM and DMM-LIPUS groups at day 1. One week after surgery, the duty cycle of right hind paw of DMM group was still impaired (Figure 1F,G). Interestingly, after one week's LIPUS treatment, the duty cycle of injured paw was ameliorated and became almost normal (Figure 1F,G). Two weeks after surgery, the right hind paw duty cycle of both DMM and DMM-LIPUS groups became

normal (Figure 1F,G). The above results suggest that LIPUS accelerates the recovery of abnormal gait pattern during the early stage of DMM model.

### **LIPUS significantly suppresses synovial inflammation in the DMM and air pouch models**

Synovitis is an important cause of abnormal gait pattern such as painful limp [24]. To further investigate whether the synovial inflammation is involved in LIPUS-mediated effects on gait pattern, all mice were sacrificed, and the injury knee joints were prepared for histologic analysis. As shown in Figure 2A, the synovial inflammation of injured joints in surgery mice were more severe than that of control mice, including more infiltrating inflammatory cells, synovial hyperplasia and loose, pannus outgrowth at the surface of bone and cartilage, and more inflammatory cells in the synovial cavity (synovial exudate). After LIPUS treatment, the synovial hyperplasia and synovial exudate severity were all alleviated (Figure 2A). We also assessed the total synovitis scores according to synovitis scoring system described before [25]. The scores in DMM surgery mice were remarkably higher compared that of the negative control mice (Figure 2B). The total synovitis scores were lower in the LIPUS treatment mice than those in DMM mice (Figure 2B). Collectively, these results indicate that LIPUS alleviates the synovitis of mice with DMM surgery.

In addition, air pouch murine model, another model for studying synovitis [26], was also utilized to check the anti-inflammatory ability of LIPUS. We injected LPS into subcutaneous air pouch to induce synovium-like inflammation. The experimental procedure for LIPUS treatment was shown in Figure 2C. The LPS injection group had thicker synovium-like tissue compared to PBS group, which was alleviated by LIPUS treatment (Figure 2D). In addition, the level of IL1B in exudates of LPS group was significantly higher than that of PBS group, which was largely reversed by LIPUS (Figure 2E). After LIPUS treatment, the thickness of synovium-like tissue became thinner (Figure 2F). Then, we checked the total cells in pouch wall and found that LPS group had more cells compared to PBS group (Figure 2G). However, there was no significant difference between LPS and LPS-LIPUS treatment groups (Figure 2G). We next checked the number of macrophage-like ADGRE1/F4/80<sup>+</sup> cells in air pouch wall (Figure 2H). The percent of ADGRE1<sup>+</sup> macrophages in LPS injection synovium was significantly higher than that of control synovium (Figure 2I). Compared with LPS group, there was no statistical change of the macrophage percentage after LIPUS treatment (Figure 2I). Taken together, the present results indicate that LIPUS suppresses LPS-induced synovitis in air pouch model, but the number of macrophages is not influenced by LIPUS.

### **LIPUS suppresses the production of mature IL1B in macrophages**

Proinflammatory mediators such as IL1B produced by the synovial macrophages contribute to clinical symptoms and cartilage breakdown in OA [3,12]. It has been reported that inflammasome-mediated production of mature IL1B plays an important role in hydroxyapatite-associated synovitis [27]. Thus, we further observed the expression of PYCARD/ASC (PYD and CARD domain containing), which is the core component of

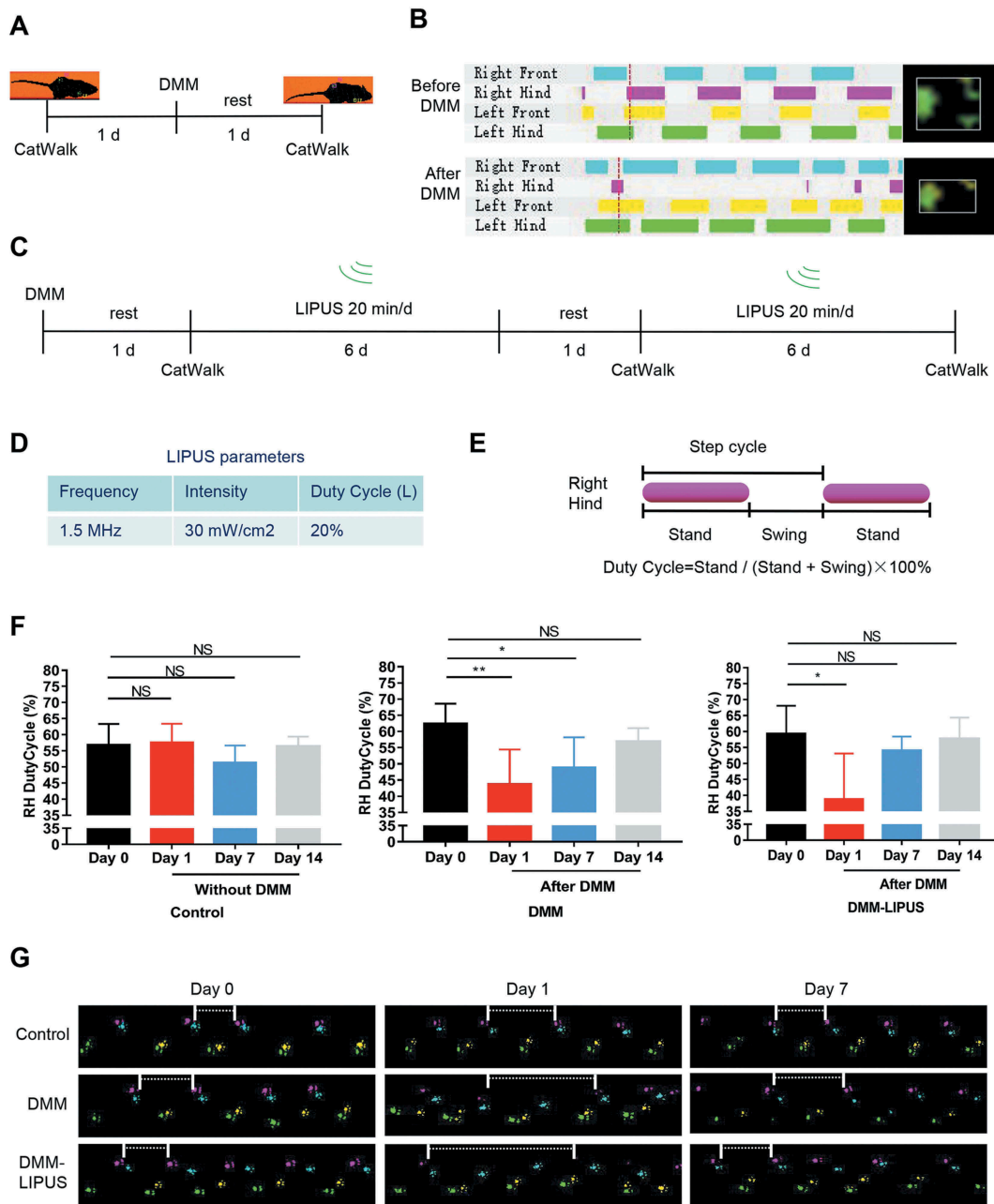


**Figure 1.** LIPUS ameliorates the pain gait patterns of mice with DMM. (A and B) CatWalk footprints were detected before and after DMM surgery. The colored bands represent standing time of each foot and the right panels are footprints of right hind paw reflected by green LED light. (C) Illustration of the protocols of LIPUS treatment and CatWalk gait analysis. (D) Three parameters of LIPUS treatment. Duty Cycle (L) represents the duty cycle of LIPUS. (E) The computational formula of duty cycle for CatWalk gait analysis. “Stand” refers to the time of duration in the contact of a paw and “Swing” refers to the duration without contact of a paw during one step cycle. (F) The duty cycle was recorded and analyzed by CatWalk software ( $n = 4$ ). RH, right hind; Statistical analyses were performed using one-way ANOVA followed by Dunnett’s multiple comparisons test. NS, not significant, \* $p < 0.05$ , \*\* $p < 0.01$ . (G) Representative footprint images were recorded during the treatment of LIPUS. The footprints of the operated right hind limbs are labeled with pink (prints of the right front limb in cyan). The paw prints of the left front limbs are yellow (prints of the left hind limb in green). The space between white short lines represent the swing phase of right hind limbs.

inflammasome and involves in the production of mature IL1B [28]. As shown in Figure 3A, numerous PYCARD-specks could be detected in OA patients-derived synovium of keen joint. In murine model, few PYCARD-positive macrophages could be found in normal synovium of joint, but there were tremendous number of PYCARD-positive macrophages in the thickened synovium of DMM surgery mice (Figure 3B). Interestingly, the number of PYCARD-positive macrophages in DMM surgery mice with LIPUS treatment was decreased, which indicated that LIPUS decreased the PYCARD level in synovial macrophages of DMM

mouse model (Figure 3B,C). The similar phenomenon was also observed in synovium of LPS induced air pouch model (Figure S1). Moreover, LIPUS treatment significantly decreased the number of cells expressing IL1B in the synovium of mice with DMM surgery (Figure 3D,E).

To further investigate the effect of LIPUS on IL1B *in vitro*, LPS plus ATP were used to treat macrophages to induce the production of mature IL1B [29]. Consistent with previous study [30], the supernatant IL1B of LPS-ATP-treated macrophages gradually increased after ATP was removed (Figure 3F), revealing that this

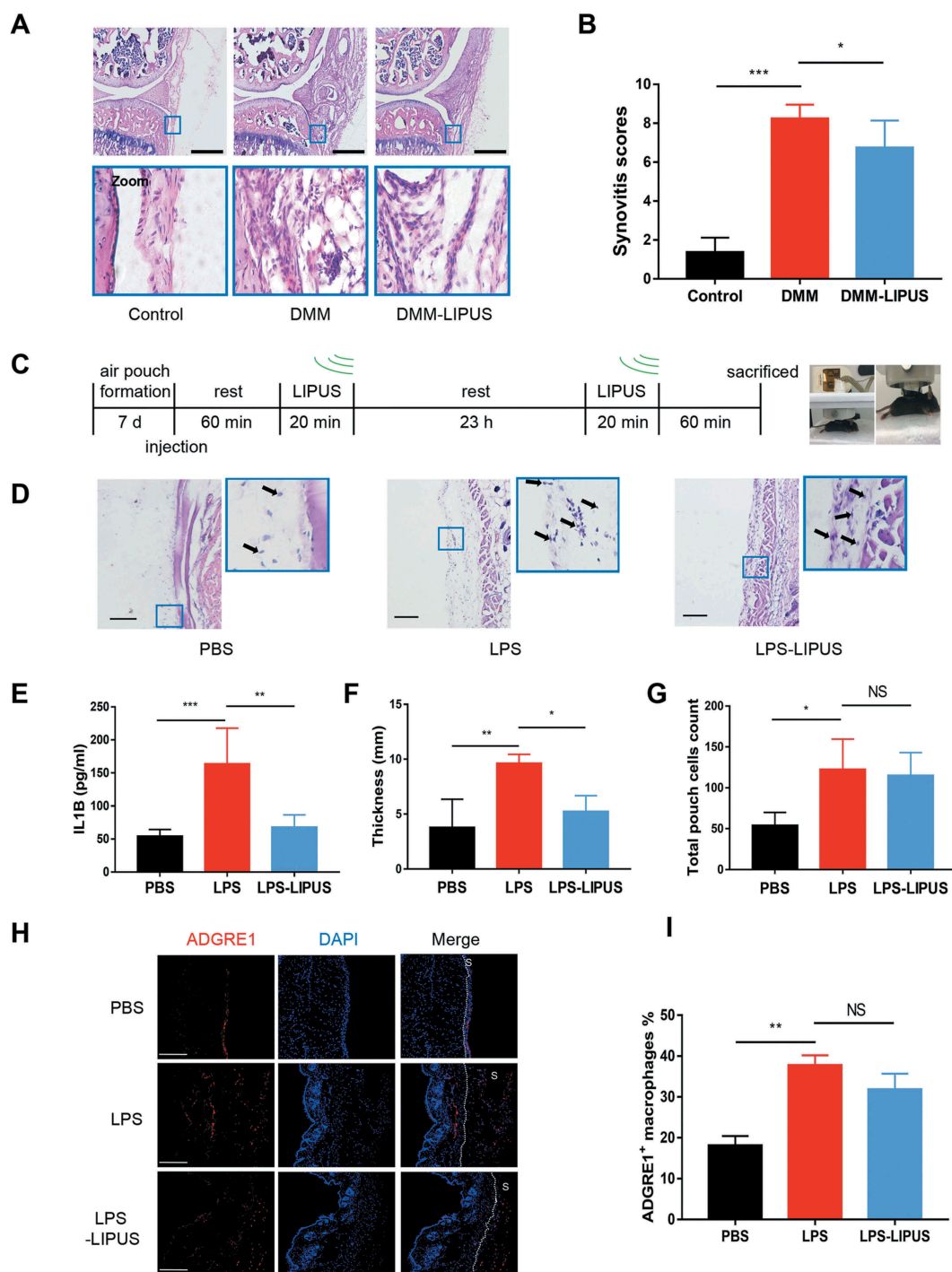


**Figure 2.** LIPUS significantly suppresses synovial inflammation in the DMM and air pouch mouse models. (A and B) Twelve mice were sent to experiment for the first time. Two weeks later, another 12 mice were sent to the same experiment. Histopathological evaluation of the medial compartment of male C57BL/6 mouse knee joints after DMM operation with or without LIPUS treatment, and the representative images were listed (A) and the total synovitis scores following DMM surgery were calculated (B). Scale bar: 100  $\mu$ m.  $n = 8$ . (C) The procedure of LIPUS treatment in LPS-induced air pouch model. The right panel shows the LIPUS device on the skin surface of air pouch. (D) Synovium-like subcutaneous air pouches of different groups were stained with H&E and black arrows represent the monocytes in the air pouch wall. Scale bars: 100  $\mu$ m. (E) Supernatants from the exudate of air pouch were collected by centrifugation. IL1B levels of supernatants were measured by enzyme-linked immunosorbent assay ( $n = 6$ ). (F, G) The thickness and total cells of air pouch wall were measured in each group. (H) The macrophages in air pouch wall were stained by anti-ADGRE1 (red staining) antibody. Nuclei were stained with DAPI (blue fluorescence). The dotted lines indicate the boundary of synovium. Scale bars: 200  $\mu$ m. (I) The percentage of ADGRE1-positive macrophages in total cells in air pouch wall is presented. S represents synovium. The above statistical analyses were performed using two-way ANOVA followed by Bonferroni's multiple comparisons test. \* $p < 0.05$ , \*\* $p < 0.01$ , \*\*\* $p < 0.001$ , NS, not significant.

model was available to investigate the role of LIPUS on IL1B. Next, we applied LIPUS after LPS-ATP exposure in macrophages and then detected the supernatant IL1B (Figure 3G). In THP-1 cells with the treatment of LPS-ATP, the level of supernatant IL1B was

remarkably downregulated by LIPUS (Figure 3H). Subsequently, we isolated and differentiated the bone marrow derived macrophages (BMDMs) from C57BL/6 mice, whose ADGRE1 is highly expressed in the cytoplasm (Figure S2). The level of supernatant

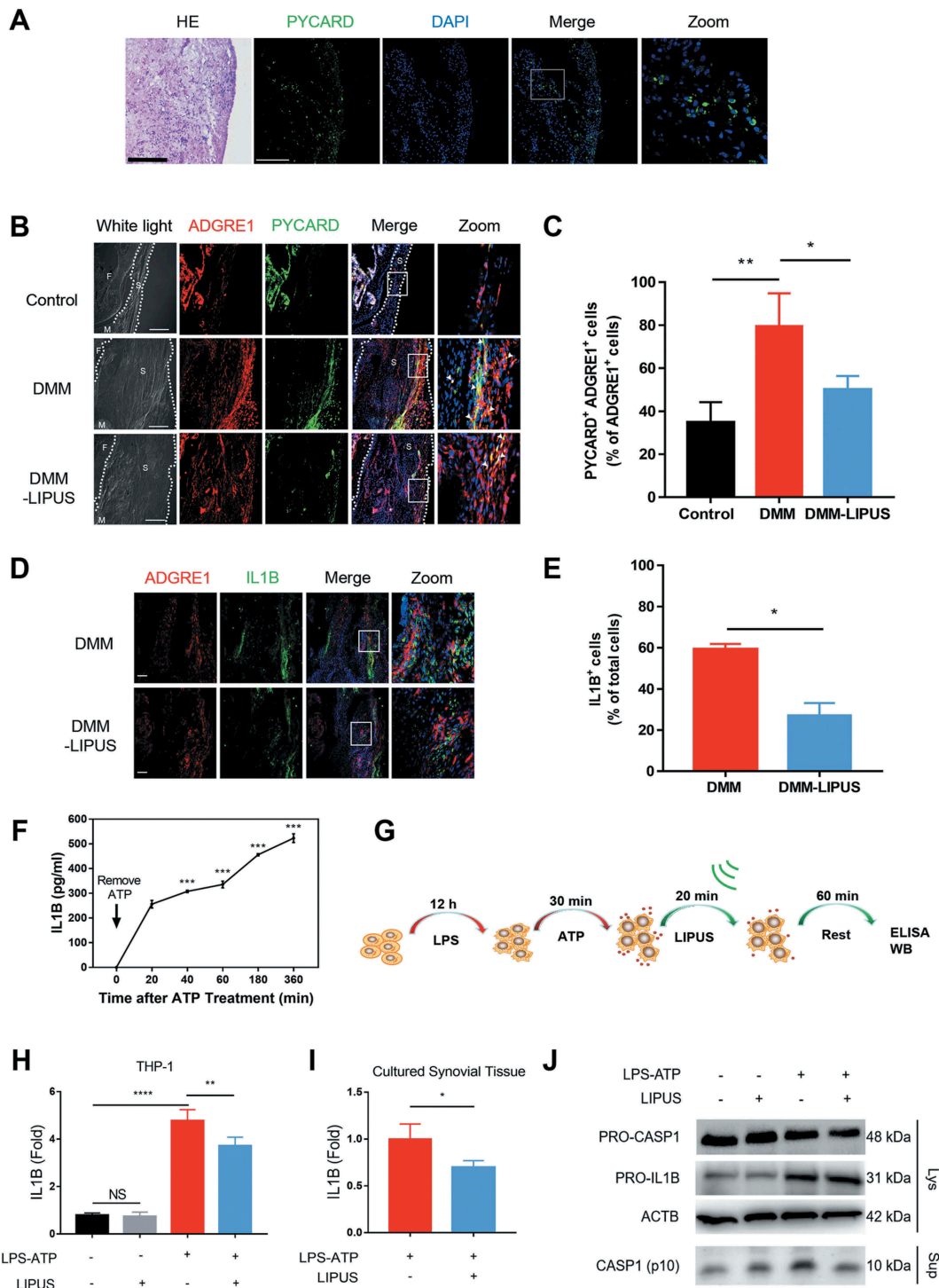


**Figure 3.** LIPUS suppresses the production of mature IL1B *in vivo* and *in vitro*. (A) Hematoxylin and eosin staining of OA patients-derived synovium (right panel). Frozen sections of OA patients' synovium were stained with anti-PYCARD (green) antibodies. Nuclei were stained by DAPI (blue). Scale bars: 200  $\mu$ m. (B) The medial compartment of right knee joint sections were stained with anti-ADGRE1 (red) and anti-PYCARD (green) antibodies. Nuclei were stained by DAPI. The white arrows represent PYCARD<sup>+</sup> macrophages. The dotted lines indicate the boundary of synovium of joint. Scale bars: 200  $\mu$ m. (C) The percentage of double (ADGRE1 and PYCARD) positive cells among the ADGRE1-positive cells in synovium. Statistical analyses were performed using two-way ANOVA followed by Bonferroni's multiple comparisons test. \* $p < 0.05$ , \*\* $p < 0.01$ . (D) The sections of right knee joint were stained with anti-IL1B (green) and anti-ADGRE1 (red) antibodies. Scale bars: 100  $\mu$ m. (E) The percentage of IL1B-positive cells among total cells in synovium. Statistical analyses were performed using Student's t test. \* $p < 0.05$ . (F) PMA-primed THP-1 cells were treated with LPS for 12 h and subsequently with ATP for 30 min. The levels of supernatant IL1B were measured at 20, 40, 60, 180 and 360 min after ATP removal. Statistical analysis was using one-way ANOVA followed by Dunnett's multiple comparisons test. \*\*\* $p < 0.001$ , compared with the IL1B level at 20 min after ATP removal. (G) Working model of treatment of LPS-ATP-LIPUS on macrophages. Briefly, macrophages were stimulated with LPS (100 ng/ml) for 12 h and subsequently treated with ATP (3 mM) for 30 min. And then exposed to LIPUS for 20 min. (H) THP-1 cells were treated by LPS-ATP, and subsequently treated with or without LIPUS treatment. Subsequently, 60 min later, the levels of supernatant IL1B in cultured medium at 60 min timepoint after LIPUS treatment were measured by ELISA. Statistical analyses were performed using two-way ANOVA followed by Bonferroni post-tests. NS, not significant, \*\* $p < 0.01$ , \*\*\*\* $p < 0.0001$ . (I) Cultured synovial tissues of OA patients were stimulated with LPS-ATP in the absence or presence of LIPUS treatment and the levels of supernatant IL1B of each group were measured by ELISA ( $n = 4$ ). Statistical analyses were performed using Student's t test. \* $p < 0.05$ . (J) After the indicated treatments, the precursors of IL1B and CASP1 in lysates and cleaved CASP1 (p10) in culture supernatants of THP-1 cells were tested using western blot. ACTB/ $\beta$ -actin was used as a loading control. M represents meniscus, T represents tibia, S represents synovium.

IL1B in LPS-ATP-treated BMDMs were significantly decreased at 60, 180 and 360 min after LIPUS treatment (Figure S3A). In order to explore whether LIPUS destroy the cytokine in a way that antibodies do not recognize their epitopes, we treated recombinant human IL1B protein at different concentrations with or without LIPUS for enzyme-linked immunosorbent assay (ELISA) assay. The data showed that the levels of supernatant IL1B were not affected by LIPUS (Figure S3B). Then the LPS-ATP-treated macrophages were treated with LIPUS in the presence or absence of MCC950, which could restrain the production of mature IL1B via inhibition of NLRP3 (NLR family pyrin domain containing 3) [31]. The results demonstrated that LIPUS did not prevent MCC950 from reducing the IL1B production induced by ATP (Figure S3C). In addition, *NLRP3* small interfering RNAs (siRNAs) were used to knockdown the *NLRP3* expression in THP-1 cells (Figure S3D). In *NLRP3*-knockdown THP-1 cells, LIPUS could not decrease the level of mature IL1B induced by LPS-ATP, which indicated that LIPUS-mediated decrease in mature IL1B was related to *NLRP3* (Figure S3E).

In addition, we used poly(dA:dT) and muramyl dipeptide (MDP) in LPS-primed THP-1 cells to observe the effects of LIPUS on production of mature IL1B. Poly(dA:dT) and MDP significantly increased the level of mature IL1B, but LIPUS did not reverse the increase of mature IL1B in these two models (Figure S4). Moreover, the level of supernatant IL1B produced by OA patients-derived synovial tissues was significantly inhibited by LIPUS (Figure 3I). As the production of mature IL1B is highly dependent on the cleavage of protease CASP1/CASPASE-1 [32], we further detected the level of cleaved CASP1 in LPS-ATP-treated cells with or without LIPUS. As shown in Figure 3J, LIPUS dramatically inhibited the protein level of cleaved CASP1 in supernatants, while had no significant effects on the expression of pro-IL1B and pro-CASP1 in lysates. In summary, the above results suggest that LIPUS inhibits the production of mature IL1B in LPS-ATP-treated macrophages.

### **The enhanced autophagy by LIPUS greatly contributes to the inhibition of mature IL1B production in LPS-ATP-treated macrophages**

Previous studies have revealed that autophagy can lead to the decreased level of mature IL1B [33–35]. Thus, we wondered that whether LIPUS-mediated inhibition of mature IL1B production was related to its regulation on autophagy flux. First, we checked the autophagy-related marker MAP1LC3B-I/II (microtubule associated protein 1 light chain 3 beta-I/II) [36] and found the protein level of LC3B-II was significantly increased by LIPUS in LPS-ATP-treated BMDMs (Figure 4A), THP-1 (Figure 4B), and Raw 264.7 cells (Figure 4C). As the increase of LC3B-II may arise from either enhanced autophagic flux or decreased autophagic degradation [36], we further used bafilomycin A<sub>1</sub> (BafA1) to inhibit lysosomal function [37] to determine the effect of LIPUS on autophagy flux. As shown in Figure 4D, LIPUS accelerated the accumulation of LC3B-II protein in BafA1-treated cells, indicating an increased autophagy flux upon LIPUS treatment. We next examined the expression pattern of endogenous LC3B upon LIPUS treatment by confocal microscopy. As shown in Figure 4E, the green signals of LC3B were distributed in the cytoplasm and nucleus (especially in nucleus) and formed some

puncta in the cytoplasm in LPS-ATP-treated cells. After the treatment of LIPUS, the signals of LC3B in nucleus were significantly decreased, while the signals of LC3B in cytoplasm and the corresponding puncta were remarkably increased, suggesting the increased autophagosomes induced by LIPUS (Figure 4E) [38]. Similar results were also observed in BMDMs from green fluorescent protein (GFP)-LC3 transgenic mice (GLM-BMDMs) (Figure S5). In order to further observe the effect of LIPUS on autophagy flux, we used a tandem monomeric red fluorescent protein (RFP)-GFP-LC3 plasmid in our study [39]. The number of autolysosomes labeled with RFP significantly increased by LIPUS treatment in LPS-ATP-treated THP-1 cells and the number of RFP puncta significantly exceeded that of GFP puncta (Figure 4F). The data indicated that the autophagy flux was not blocked in LPS-ATP-treated macrophages with or without LIPUS treatment. Moreover, transmission electron microscopy (TEM) was used to check the number of autophagic vacuoles. TEM showed that there were some autophagic vacuoles within the cytoplasm in THP-1 cells following LPS-ATP treatment, while more autophagic vacuoles could be observed after LIPUS treatment (Figure 4G). To evaluate the effect of LIPUS on autophagy *in vivo*, we treated GFP-LC3 transgenic mice with LIPUS in air pouch murine model (Figure 4H). As shown in Figure 4I, LPS injection group had more GFP-LC3-positive cells in synovium-like tissue than control group, while LIPUS increased the number GFP-LC3-positive cells after LPS injection.

Next, we used PI3K inhibitor 3-methyladenine (3-MA) [40] and siRNAs of *ATG7* (autophagy-related 7) to inhibit autophagy in THP-1 cells so as to investigate the effect of LIPUS-enhanced autophagy on mature IL1B production. As shown in Figure 4J, there was no significant difference of mature IL1B level in 3-MA-pretreated cells between LPS-ATP and LPS-ATP-LIPUS groups. After the efficient interference of *ATG7* (Figure S6), the level of supernatant IL1B was significantly increased in THP-1 cells, while the inhibitory effect of LIPUS on mature IL1B production was eliminated (Figure 4K). In brief, the above results suggest that LIPUS inhibits production of mature IL1B by enhancing autophagy flux in LPS-ATP-treated macrophages.

### **The enhanced autophagy by LIPUS facilitates degradation of SQSTM1 in LPS-ATP-treated macrophages**

The previous studies revealed that SQSTM1 can be degraded through autophagy [41]. In addition, the protein level of SQSTM1 is tightly involved in production of mature IL1B *in vitro* and *in vivo* [33,42,43]. As LIPUS dramatically promoted autophagy in LPS-ATP-treated macrophages, we conjectured whether the effect of LIPUS-enhanced autophagy on production of mature IL1B was related to SQSTM1. Firstly, we detected the change of SQSTM1 protein level by western blot. The protein level of SQSTM1 was significantly downregulated by LIPUS in LPS-ATP-treated THP-1 cells (Figure 5A), BMDMs (Figure S7A) and Raw 264.7 cells (Figure S7B). Next, we used cycloheximide (CHX) to inhibit protein synthesis in LPS-ATP-treated THP-1 cells and then estimated the effect of LIPUS on SQSTM1 level. As shown in Figure 5B, LIPUS still downregulated the protein level of SQSTM1 in THP-1 cells after the protein synthesis was blocked, indicating that the degradation at protein level was an important mechanism for LIPUS-regulated SQSTM1. Moreover, lysosomal inhibitor

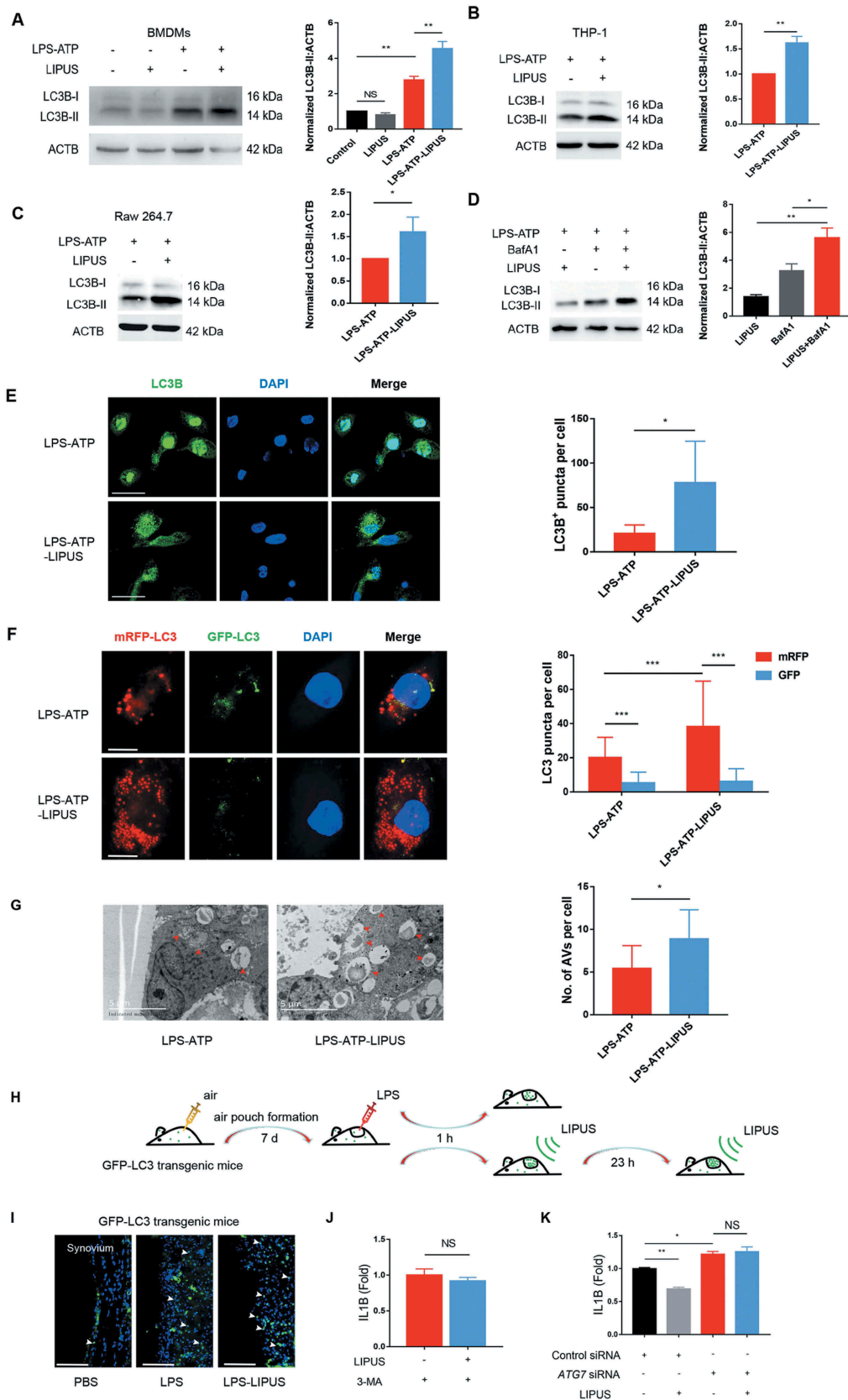


**Figure 4.** The enhanced autophagy contributes to LIPUS-mediated inhibition on the production of mature IL1B in LPS-ATP treated macrophages. BMDMs (A), THP-1 cells (B) and Raw 264.7 cells (C) with the indicated treatments were subjected to western blot assay using anti-LC3B antibody and anti-ACTB antibody. Statistical analysis (A) was performed using two-way ANOVA followed by Bonferroni's multiple comparisons test. NS, not significant,  $^{***}p < 0.01$ . Statistical analyses (B and C) were performed using Student's t test.  $^{*}p < 0.05$ ,  $^{***}p < 0.01$ . (D) THP-1 cells were treated by LPS-ATP in the absence of 100 mM BafA1 with or without LIPUS at the same time. 3 h later, the protein level of LC3B was analyzed by western blot. Statistical analysis was performed using two-way ANOVA followed by Bonferroni's multiple comparisons test.  $^{*}p < 0.05$ ,  $^{***}p < 0.01$ . (E) THP-1 cells with the indicated treatments were stained with anti-LC3B (green) and DAPI (blue). The numbers of LC3 puncta were counted in six different arbitrary areas (the right panel). Scale bars: 50  $\mu$ m. Statistical analyses were performed using Student's t test.  $^{*}p < 0.05$ . (F)

BafA1 reversed the effect of LIPUS on SQSTM1 protein level, indicating LIPUS decreases SQSTM1 protein level mainly via autophagy pathway (Figure 5C). To further investigate the role of autophagy in this process, we treated THP-1 cells with specific *ATG7* siRNAs to inhibit the autophagy flux. As shown in Figure 5D, the accumulated SQSTM1 resulting from ATP/LPS treatment was not decreased by LIPUS in *ATG7*-KD cells. Moreover, we used immunofluorescence assay to observe the change of endogenous SQSTM1 under confocal microscopic. As shown in Figure 5E, LPS-ATP treatment significantly increased number of SQSTM1 puncta in THP-1 cells, which could be decreased after LIPUS treatment. These data reveal that LIPUS-enhanced autophagy facilitates the degradation of SQSTM1 in LPS-ATP-treated macrophages.

### **Autophagy-dependent degradation of SQSTM1 is important for the LIPUS-mediated inhibition of mature IL1B production in LPS-ATP-treated macrophages**

To further evaluate the role of SQSTM1 in the inhibitory effect of LIPUS on mature IL1B production, we used specific siRNAs to knockdown *SQSTM1* in THP-1 cells (Figure 6A). LIPUS had no significant effect on the level of mature IL1B in *SQSTM1*-KD cells after LPS-ATP treatment (Figure 6B). Next, we created the plasmid overexpressing SQSTM1 (CMV-SQSTM1-eGFP) and another plasmid carrying point mutations (D335A D336A D337A) in the LC3-interacting region (LIR) of SQSTM1 (CMV-SQSTM1<sup>D335,336,337A</sup>-eGFP), which could abolish the interaction of SQSTM1 with LC3 (Figure 6C) [44]. The level of supernatant IL1B was significantly decreased after SQSTM1 was overexpressed in LPS-ATP-treated macrophages (Figure 6D). Compared with the control plasmid (CMV-SQSTM1-eGFP), the level of supernatant IL1B was increased after transfection of mutant LIR plasmid in LPS-ATP-treated THP-1 cells (Figure 6D). In addition, LIPUS failed to inhibit the production of supernatant IL1B in *SQSTM1* mutant cells (Figure 6E). Moreover, LIPUS treatment dramatically decreased the level of ubiquitinated proteins in macrophages (Figure 6F). As SQSTM1 recruits ubiquitinated proteins to autophagosome and delivers the cargo to lysosome for degradation [45], we deduced that SQSTM1-dependent autophagic degradation of ubiquitinated proteins may be an important mechanism for LIPUS-mediated effects on macrophages. Taken together, the above results suggest that LIPUS suppresses LPS-ATP-induced production of mature IL1B in macrophages through autophagy-mediated degradation of SQSTM1.

### **LIPUS promotes the formation of SQSTM1-PKM complex and the degradation of PKM in an autophagy-dependent way**

Next, we used the combined experiments of immunoprecipitation and mass spectroscopy (IP-MS) to screen the potential proteins that may mediate the anti-inflammatory effect of LIPUS (Figure 7A–C). Interestingly, pyruvate kinase was screened out with a high score in SQSTM1-immunoprecipitates. Recently, PKM2 (one of the four pyruvate kinase isoforms) has been discovered to play an important role in regulation of inflammation [46]. Moreover, pharmacological and genetic inhibition of PKM significantly promotes the production of mature IL1B in LPS-ATP-treated macrophages [47]. Therefore, we deduced that PKM may be a novel target of SQSTM1 that contributes to the anti-inflammatory effect of LIPUS. Immunoprecipitation experiments in THP-1 cells revealed that SQSTM1 and PKM were co-existed in one complex, especially under the condition of LIPUS treatment (Figure 7D,E). The fluorescent imaging from confocal microscope also demonstrated that LIPUS treatment promoted the colocalization of SQSTM1 and PKM in cytoplasm in LPS-ATP-treated cells (Figure 7F). Moreover, LPS-ATP increased the protein level of PKM in THP-1 cells, which is partially reversed by the treatment of LIPUS (Figure 7G). In addition, the data from CHX-treated cells revealed that protein degradation was a primary way for LIPUS-mediated decrease of PKM level (Figure 7H). After *ATG7* was knockdown by siRNAs, the protein level of PKM was enhanced in LPS-ATP-treated macrophages, which suggested autophagy contributes to the PKM degradation in this condition (Figure 7I). Furthermore, the inhibitory effect of LIPUS on PKM protein level was abolished in THP-1 cells after *ATG7* knockdown, suggesting that LIPUS decreased the level of PKM mainly through autophagy pathway (Figure 7I). Moreover, LIPUS no longer downregulated the protein level of PKM after *SQSTM1* knockdown (Figure S8), suggesting that *SQSTM1* was essential for LIPUS-mediated PKM degradation in LPS-ATP-treated macrophages. In summary, PKM is a novel target of SQSTM1, which could be downregulated by LIPUS via autophagy-mediated degradation.

Next, we evaluated the effect of LIPUS on the PKM level in synovial macrophages of mice with DMM surgery *in vivo*. The therapeutic procedure of LIPUS for DMM mice were shown in Figure 7J. The protein level of PKM in synovial macrophages were dramatically increased after DMM surgery, while it could be

---

Confocal images of THP-1 cells stably expressing mRFP-GFP-LC3. Scale bars: 20  $\mu$ m. 40 cells from each group were counted (the right panel). Statistical analysis was performed using two-way ANOVA followed by Bonferroni's multiple comparisons test. \*\*\* $p < 0.001$ . (G) TEM was used for detection of autophagic vacuoles formation in THP-1 cells with LPS-ATP or LPS-ATP-LIPUS treatment. Red arrowhead indicates an AV (autophagic vacuole). The right panel is the quantification of number of AVs per cell. The number of AVs was counted in nine different arbitrary areas. Scale bars: 5  $\mu$ m. Statistical analyses were performed using Student's t test. \* $p < 0.05$ . (H and I) LPS-induced air pouch model of synovitis was generated in GFP-LC3 transgenic mice. After LPS injection, the mice were treated with LIPUS twice. 24 h later, the synovium-like tissue in skin was prepared for fluorescent microscopy. Nuclei were stained by DAPI (blue fluorescence). The white arrows represent GFP-positive cells. Scale bar: 100  $\mu$ m. (J) LPS-ATP-treated THP-1 cells were treated with 3-MA (2 mM) in the presence or absence of LIPUS treatment and subsequently IL1B levels were measured. Statistical analysis was performed using Student's t test. NS, not significant. (K) THP-1 cells were transfected with *ATG7* siRNA (1) to knock down *ATG7* for 24 h and then given the treatments indicated. The level of IL1B in supernatants was detected by ELISA. Statistical analysis was performed using two-way ANOVA followed by Bonferroni's multiple comparisons test. NS, not significant, \* $p < 0.05$ , \*\*\* $p < 0.01$ .



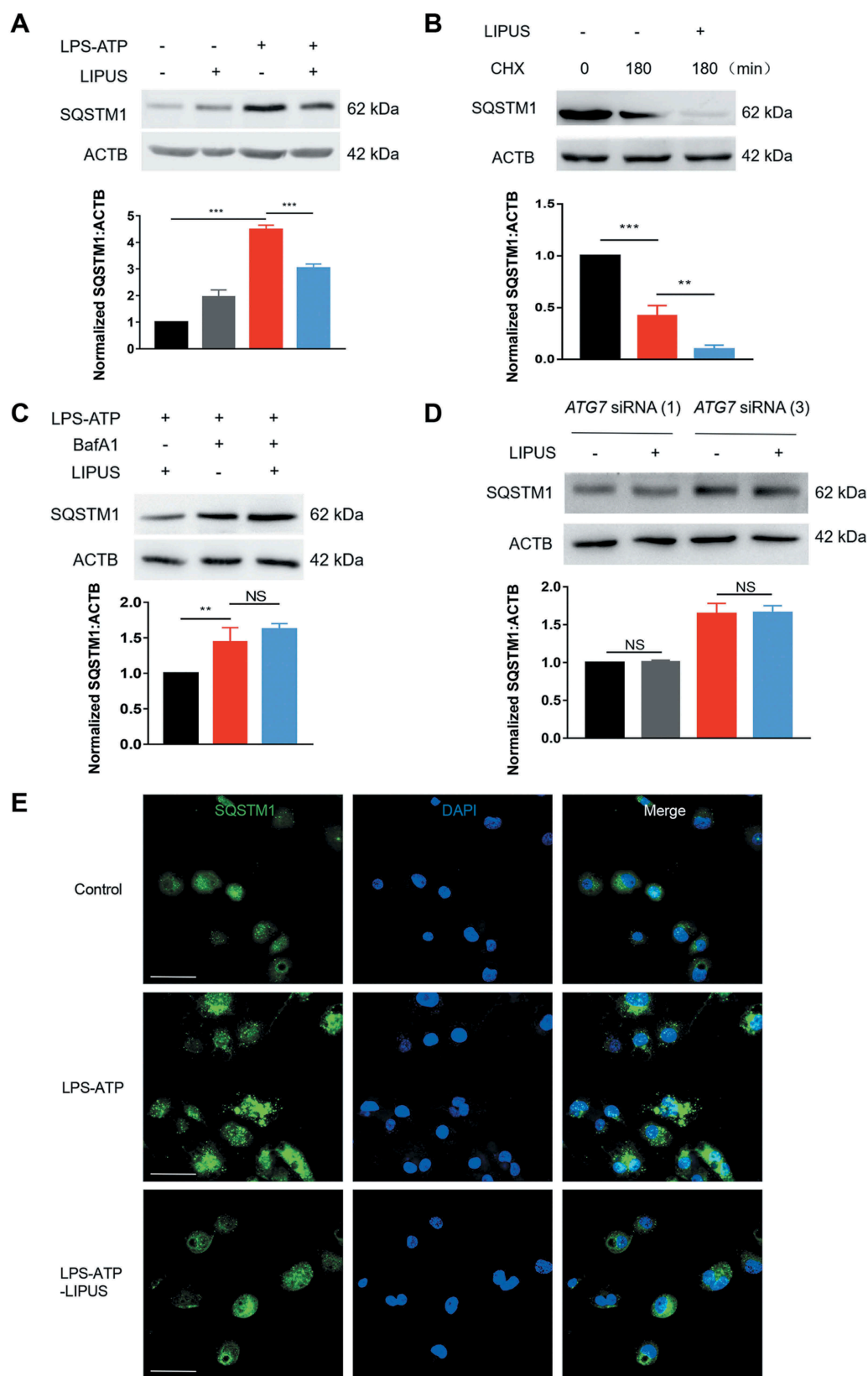


**Figure 5.** The facilitated degradation of SQSTM1/p62 by LIPUS was highly dependent on autophagy. (A) THP-1 cells were treated by LPS for 12 h and ATP for 30 min, and then exposed to LIPUS for 20 min. Sixty min later, the protein level of SQSTM1 was detected by western blotting. Statistical analysis was performed using two-way ANOVA followed by Bonferroni's multiple comparisons test.  $***p < 0.001$ . (B) LPS-ATP-treated THP-1 cells were treated with 5  $\mu\text{M}$  CHX for 180 min with or without LIPUS and then the SQSTM1 level was detected by western blotting. Statistical analysis was performed using two-way ANOVA followed by Bonferroni's multiple comparisons test.  $**p < 0.01$ ,  $***p < 0.001$ . (C) LPS-ATP-treated THP-1 macrophages were exposure to LIPUS in the absence or presence of 100 nM BafA1 and then SQSTM1 were examined by western blotting. Statistical analysis was performed using two-way ANOVA followed by Bonferroni's multiple comparisons test. NS, not significant,  $**p < 0.01$ . (D) After ATG7 knockdown, the protein level of SQSTM1 in LPS-ATP or LPS-ATP-LIPUS-treated THP-1 cells was analyzed by immunoblotting. ACTB was used as control. Statistical analyses were performed using Student's t test. NS, not significant. (E) THP-1 cells were given the indicated treatments and then the colocalization SQSTM1 (green) were detected under the fluorescent microscope. DAPI (blue). Scale bars: 20  $\mu\text{m}$ .

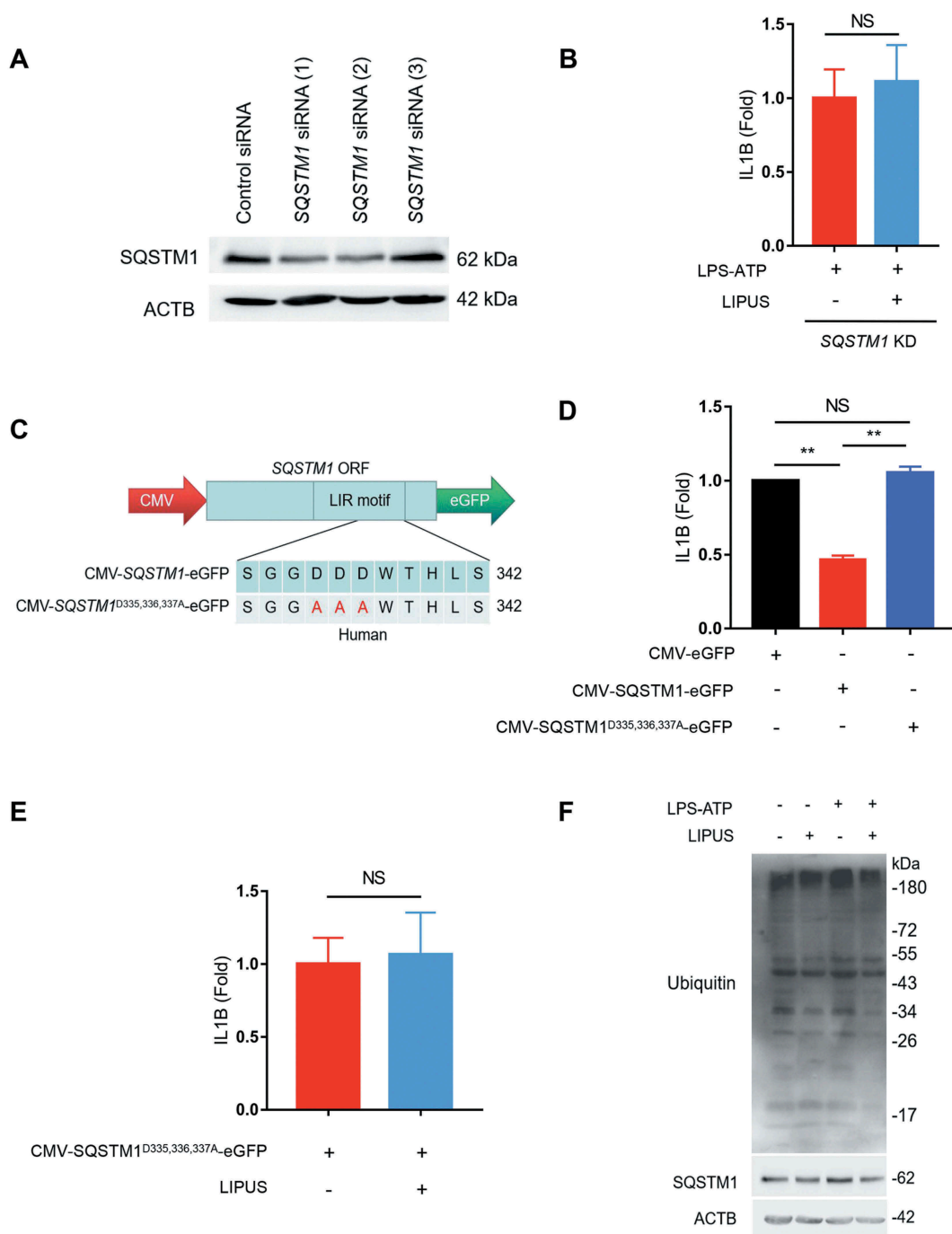


**Figure 6.** Autophagy-dependent degradation of SQSTM1 contributes to LIPUS-mediated inhibition of mature IL1B production. (A) Specific *SQSTM1* siRNAs were used to knockdown SQSTM1 level. (B) After pretreatment with *SQSTM1* siRNA (1) for 24 h, the THP-1 cells were treated with LPS (12 h) and ATP (30 min) and then treated with or without LIPUS (20 min). Sixty min later, the mature IL1B level was examined by ELISA. (C) Diagrams of the indicated plasmids for exogenous expression of SQSTM1 (CMV-SQSTM1-eGFP) and its mutant (CMV-SQSTM1<sup>D335,336,337A</sup>-eGFP). (D) THP-1 cells were transfected with CMV-SQSTM1-eGFP and CMV-SQSTM1<sup>D335,336,337A</sup>-eGFP plasmids for 24 h and then treated with LPS (12 h) plus ATP (30 min). One hour later, the levels of IL1B in supernatants were examined by ELISA. CMV-eGFP plasmid was used as the control. (E) CMV-SQSTM1<sup>D335,336,337A</sup>-eGFP plasmid was transfected into THP-1 cells for 24 h and the cells were then exposed to LPS-ATP with or without LIPUS treatment. The release of mature IL1B was tested by ELISA assay. (F) Using anti-ubiquitin and anti-SQSTM1 antibody, western blotting analyses for THP-1 cells that treated with LPS (12 h), ATP (30 min) with or without LIPUS (20 min). The above statistical analyses were performed using Student's t test. NS, not significant, \*\**p* < 0.01.

decreased by LIPUS treatment (Figure 7K). These data further revealed that LIPUS alleviated the PKM level of synovial macrophages, suggesting a potential role of LIPUS-regulated PKM in synovitis.

As shown in Figure 8, LIPUS treatment ameliorates the synovial inflammation and abnormal gait patterns in animal

models. Mechanistically, LIPUS significantly enhances the autophagy flux and increases the formation of SQSTM1-PKM complex, which promote the autophagic degradation of PKM in a SQSTM1-dependent manner that ultimately inhibits the production of mature IL1B in synovial macrophages.

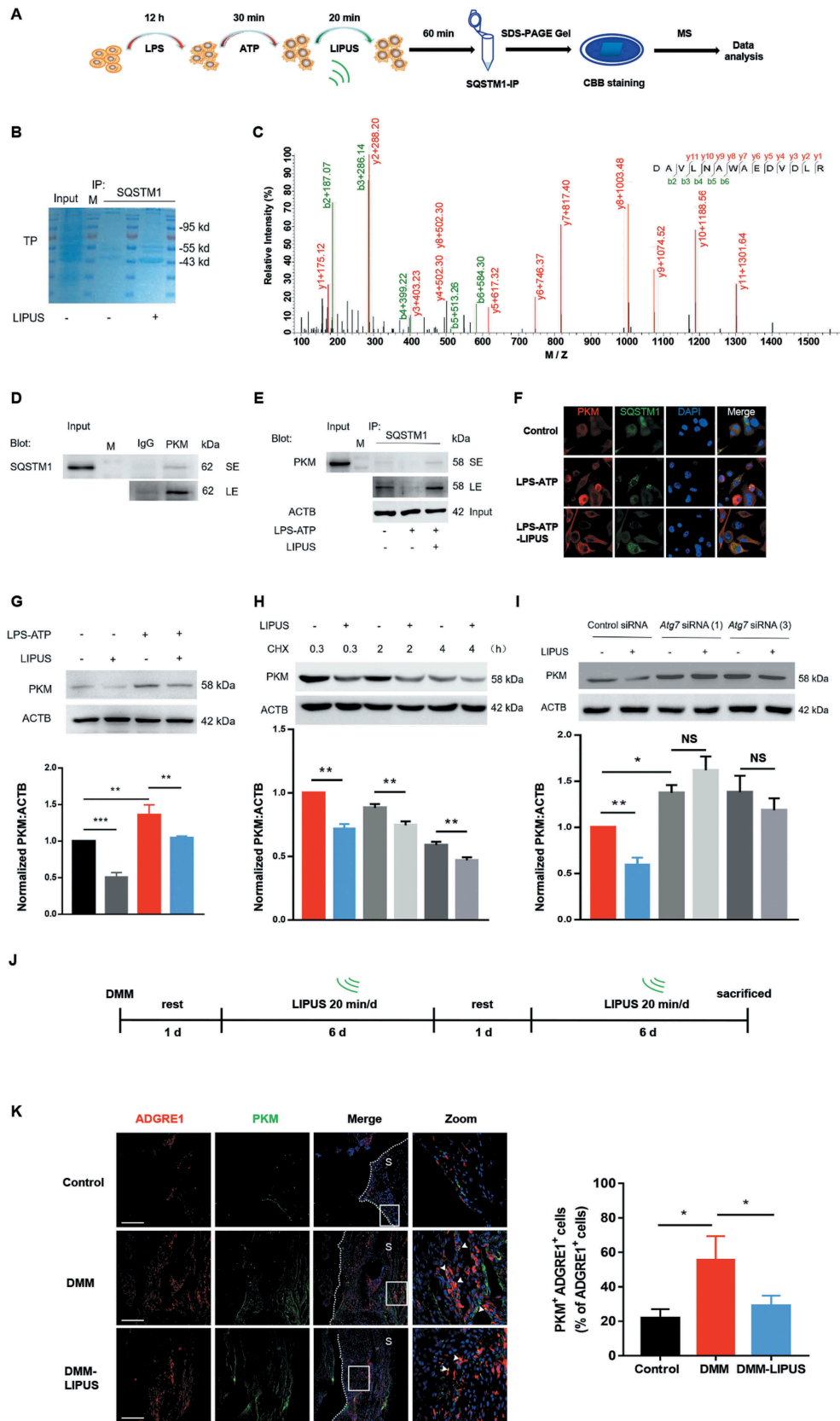


**Figure 7.** LIPUS accelerates the formation of SQSTM1-PKM complex and promotes the degradation of PKM in an autophagy-dependent way. (A) THP-1 cells were stimulated with LPS for 12 h and ATP for 30 min. Then, the cells were treated with or without LIPUS for 20 min. Sixty min later, the cells were harvested for immunoprecipitation (IP) with SQSTM1. Then, the immunoprecipitates were subjected to SDS-PAGE gel and stained with Coomassie Brilliant Blue (CBB). Subsequently, the gel was cut and subjected to mass spectrometry analysis. (B) CBB staining for SQSTM1-immunoprecipitates in SDS-PAGE gel. (C) The mass spectrum of peptides for PKM is shown. (D) THP-1 cell lysates were immunoprecipitated with anti-PKM antibodies and subsequently immunoblotted with anti-SQSTM1 antibodies. (E) THP-1 cells were exposed to LPS for 12 h and ATP for 30 min. Subsequently, LIPUS treated cells for 20 min. Sixty min later, whole cell lysates were collected for immunoprecipitation with anti-SQSTM1 antibody and immunoblotted with anti-PKM antibody. (F) Immunostaining detection for PKM (red) and SQSTM1 (green) in LPS-ATP or LPS-ATP-LIPUS-treated THP-1 cells. Scale bars: 20  $\mu$ m. (G) After THP-1 cells were treated with or without LPS-ATP and LIPUS, the lysates were obtained for western blotting assays with anti-PKM antibodies. Statistical analysis was performed using two-way ANOVA followed by Bonferroni's multiple

## Discussion

Synovium is an essential component of synovial joint, whose inflammation has been considered to be tightly associated with joint pathology and function. Targeting synovial inflammation for the treatment of joint-related diseases including OA has aroused great interest in recent years [3,11]. However, almost all of the reported strategies need to deliver drugs via intra-articular injection so as to alleviate the synovial inflammatory response [48]. These mini-invasive operations may increase the medical costs and the pain of patients, even increase the risk of joint infection [49]. Therefore, developing noninvasive methods for synovial inflammation therapy would be more ideal for patients. Here, we first evaluated the effect of LIPUS on synovial inflammation in different animal models. Similar with the anti-inflammation role of ultrasound in other models [50,51], we found that LIPUS ameliorated synovial inflammation and improved the gait patterns in the early inflammation phase of DMM surgery model, while it also inhibited LPS-induced synovitis in air pouch model of mice. In addition, more research is needed to estimate the roles of LIPUS with different parameters to optimize the therapeutic effects.

IL1B is considered as one of the proinflammatory cytokines, which is highly associated with inflammatory pain [52,53]. IL1B promotes the endogenous release of eicosanoid, which can cause persistent mechanical nociceptor hypersensitivity [52]. Intraarticular injection of IL1RN/IL-1Ra (interleukin 1 receptor antagonist) could alleviate pain of acute anterior cruciate ligament knee injury [54]. Therefore, inhibition of the production of mature IL1B in macrophages may be a potential way for the management of joint pain. The production of mature IL1B is derived from the processing of pro-IL1B by cleaved CASP1 [55], which further is released from cytoplasmic membrane. In this study, our data showed that LIPUS inhibited the cleavage of CASP1 and the production of mature IL1B in LPS-ATP-treated macrophages. After pharmacological and genetic inhibition of NLRP3, LIPUS could not any more decrease the production of mature IL1B triggered by ATP, indirectly indicating that this effect could be related to NLRP3 in our model. Recently, several studies also reported the close association between NLRP3 inflammasome and OA, especially in synovial tissue [56], which further supports the possibility of LIPUS for OA treatment. In addition, alternative mechanisms other than inflammasome activation such as the release of mature IL1B should be considered for LIPUS-mediated effect on IL1B [32,57]. More research is needed to investigate the details in the future.

SQSTM1 has an ubiquitin-associated (UBA) domain to recognize ubiquitinated protein [58]. Besides, LIR of SQSTM1 contributes to its autophagy degradation [44]. As a receptor protein, SQSTM1 binds to autophagic effector proteins LC3B to promote

ubiquitinated protein degradation [59]. Assembled inflammasomes recruit SQSTM1 to assist the entrance of inflammasome component such as PYCARD and phosphorylated NLRP3 to autophagosomes [33,60]. The secretion of IL1B is significantly increased in SQSTM1 knockout macrophages after LPS treatment [61]. ATG16L1 (autophagy related 16 like 1) inhibits signaling of IL1B by promoting degradation of SQSTM1 via proteasomal and lysosomal pathway [62]. NF- $\kappa$ B/NF- $\kappa$ B exerts its anti-inflammatory ability by delaying the accumulation of SQSTM1 [61]. In monosodium urate crystal-induced inflammation model, SQSTM1 accumulation by impaired degradation causes amplified inflammatory responses [42]. These results suggest that the degradation of SQSTM1 is important for maintaining inflammatory signals including IL1B. In this study, we identified that autophagy-dependent degradation of SQSTM1 greatly contributes to LIPUS-decreased mature IL1B, which may provide a new strategy for the diseases with disturbance of SQSTM1 degradation.

PKM can be polyubiquitinated by EPM2A/laforin-NHLRC1/malin complex or PRKN/parkin [63,64]. Besides, the degradation of PKM is regulated by CHIP in ovarian carcinoma, in which CHIP functions as an E3 ligase to ubiquitinate PKM [65]. SQSTM1 has UBA domain to regulate the clearance of ubiquitinated proteins [66]. Since PKM can be ubiquitinated, it is possible that SQSTM1 may assist the entrance of PKM into autophagosomes for degradation. In addition, there is evidence showing that SQSTM1 can bind non-ubiquitinated proteins through its PB1 domain and then assists the selective autophagic clearance [58]. In ATG7-knockdown or SQSTM1-knockdown macrophages, LIPUS was no longer able to accelerate the degradation of PKM protein, suggesting that the degradation of PKM by LIPUS depends on autophagy and SQSTM1. However, it is still not clear whether the ubiquitination of PKM contributes to its degradation in this process. Thus, more studies are needed to explore the details of PKM degradation in macrophages. In addition, the detailed mechanism for LIPUS-accelerated formation of SQSTM1-PKM complex in macrophages remains to be explored in future. Furthermore, the roles and mechanisms of PKM on IL1B expression, processing and release may vary under different conditions. Palsson-McDermott et al. showed that LPS-induced PKM could form a complex with HIF1A/HIF-1 $\alpha$ , which further binds to the IL1B promoter and influences the expression of pro-IL1B [67]. Xie et al. reported that inhibition of PKM in LPS-ATP-treated macrophages could reduce the supernatant IL1B level but not the cellular pro-IL1B, suggesting PKM mainly affects IL1B processing in their study [47]. In our study, only the supernatant IL1B but not the protein level of cellular pro-IL1B in LPS-ATP-treated macrophages was reduced by LIPUS, indicating that LIPUS may affect the mature IL1B production but not

comparisons test. NS, not significant, \*\* $p < 0.01$ , \*\*\* $p < 0.001$ . (H) The LPS-ATP-treated cells were treated with 5  $\mu$ M CHX combined with or without LIPUS at indicated intervals. PKM expression was analyzed by western blotting. Statistical analyses were performed using Student's  $t$  test. \*\* $p < 0.01$ . (I) ATG7 siRNA (1) and (3) were transfected into THP-1 cells for 24 h to knockdown ATG7 and then the cells were treated with LPS-ATP followed with or without LIPUS. PKM level was examined by immunoblotting. Statistical analyses were performed using Student's  $t$  test. NS, not significant, \* $p < 0.05$ , \*\* $p < 0.01$ . (J) Illustration of the procedure of LIPUS treatment in DMM model. (K) The sections from right knee joint of mice were immunostained with anti-ADGRE1 (red) and anti-PKM (green) antibodies. Nuclei were stained by DAPI (blue). The white arrows refer to PKM<sup>+</sup> macrophages. Scale bars: Scale bars: 200  $\mu$ m. The percentage of PKM-positive macrophages in total ADGRE1-positive macrophages in air pouch wall is presented in right panel. Statistical analyses were performed using two-way ANOVA followed by Bonferroni's multiple comparisons test. \* $p < 0.05$ . The dotted lines represent the boundary of synovium. TP, total protein, M, marker, S, synovium.

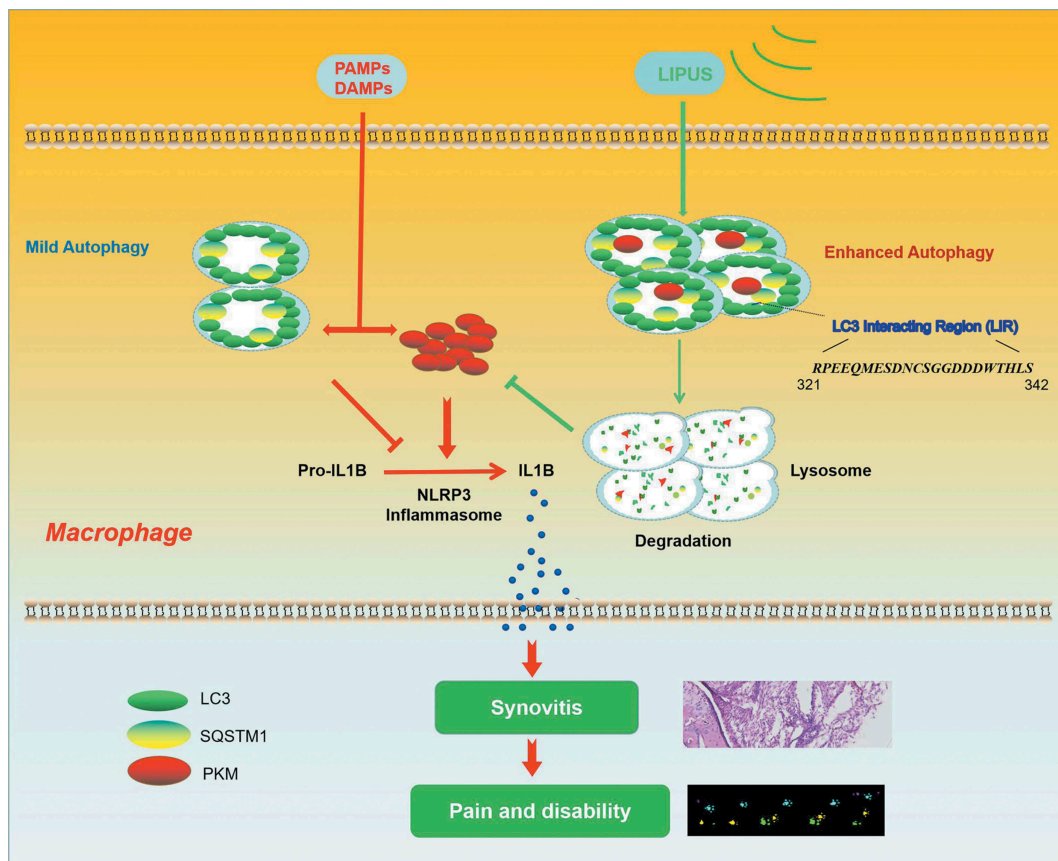


Figure 8. Working model.

the expression of pro-IL1B. More investigations are needed to study the details in the future.

In conclusion, our present study showed that LIPUS ameliorated the gait patterns and synovial inflammation in mouse models, which may be related to LIPUS-inhibitory mature IL1B production. As to the molecular mechanism, LIPUS decreased the production of mature IL1B mainly through enhancing autophagy-mediated degradation of PKM and SQSTM1 in macrophages. Our data unveil a novel mechanism for the anti-inflammatory effect of LIPUS and provide new data for the development of non-invasive treatments of inflammation-related diseases like OA.

## Materials and methods

### Cell culture

Human THP-1 monocytes (ATCC, TIB-202) and RAW 264.7 cells (ATCC, TIB-71) were maintained in  $\alpha$ -MEM medium (Gibco, 12,571,048) containing 10% fetal bovine serum (Gibco, 16,140,063) and 1% penicillin-streptomycin (Gibco, 15,140,163). All THP-1 monocytes were treated with 100 ng/ml phorbol-12-myristate-13-acetate (PMA; Sigma-Aldrich, P1585) for 72 h to differentiate into macrophages. Bone marrow cells were flushed out with  $\alpha$ -MEM medium from tibias and femurs of C57BL/6 mice (Daping Hospital Laboratory Animal Center, China) and cultured at least 6 d with 100 ng/ml recombinant murine CSF1/

M-CSF (PeproTech, 315-02) in  $\alpha$ -MEM medium to obtain BMDM.

### LPS, ATP and LIPUS treatment

The clinical LIPUS exposure system (Smith & Nephew, Exogen 4000+) was employed. The parameters of LIPUS were 1.5 MHz, 20% duty cycle (L) and 30 mW/cm<sup>2</sup> as well as therapeutic parameters in clinic. The probes of LIPUS exposure system were fixed in the bottom of 3.5 cm dish or 6-well plate covered by coupling gel. Macrophages were treated with LPS (Sigma-Aldrich, L8274) at 100 ng/mL for 12 h and then ATP (Sigma-Aldrich, 10,519,979,001) at 3 mM for 30 min. Before LIPUS treatment, the cells were washed with PBS (Solarbio, P1010) and added fresh culture medium. The cells were exposed to LIPUS for 20 min and supernatants or lysates were harvested at different times. To inhibit autophagic flux, 100 nM bafilomycin A<sub>1</sub> (BafA1; Sigma-Aldrich, B1793) or 2 mM PI-3K inhibitor 3-methyladenine (3-MA; Selleck Chemicals, S2767) was used. 5  $\mu$ g/ml CHX (Sigma-Aldrich, C7698) was used to inhibit the expression of protein.

### Synovial tissues of osteoarthritis patients and treatment

Synovial tissues were obtained from patients underwent total knee replacement because of serious OA. Patients were fully informed about the aim of this research, and the ethics approval was granted by the Ethics Committee of Southwest Hospital

(Chongqing, China). Briefly, we removed the synovial tissues from isolated knee joint carefully. Each specimen from the same area was cut into four identical parts (nature control, LIPUS, LPS-ATP, LPS-ATP-LIPUS), and cultured in  $\alpha$ -MEM medium for 3 d. At day 4, we treated specimens with LPS-ATP or LPS-ATP-LIPUS as the same way we treated cells before. The release of IL1B in supernatant was detected by human IL1B ELISA Kit. After the supernatants were collected, the synovial tissues were immediately preserved by liquid nitrogen for tissue histology.

## ELISA

IL1B in supernatants were quantified using mouse IL1B ELISA Kit (Beyotime Biotechnology, PI301) or human IL1B ELISA Kit (Beyotime Biotechnology, PI305) according to the manufacturer's instruction.

## Western blotting and immunoprecipitations

Equal amounts of protein samples were loaded on a 12% SDS-PAGE gel and transferred onto a PVDF membrane (Millipore, IPVH00010). After blocking with 5% nonfat milk in PBST (PBS (Solarbio, P1010) + 0.1% Tween-20) for 1–1.5 h, the membrane were incubated with primary antibodies specific for CASP1 (Cell Signaling Technology, 2225), IL1B (Cell Signaling Technology, 12242), ACTB/ $\beta$ -actin (Sigma-Aldrich, A8481), Cleaved CASP1 (Cell Signaling Technology, 4199), LC3B (Cell Signaling Technology, 3868), SQSTM1 (Cell Signaling Technology, 8025), ATG7 (Cell Signaling Technology, 8558), Ubiquitin (Santa Cruz Biotechnology, sc-8017), PKM/PKM2 (Proteintech, 60268-1-Ig) overnight at 4°C. HRP-conjugated secondary anti-rabbit or anti-mouse antibodies were applied for 1 h at 37°C. After washing with PBST, the signal was detected using ChemiScope 6000 (Clinx Science Instruments, China). For immunoprecipitation, whole cell lysates were incubated with anti-human SQSTM1 or PKM on a rocker at 4°C overnight and then incubated with protein A/G plus-agarose (Santa Cruz Biotechnology, sc-2003) at room temperature for 2 h. After washing 5 times with lysis buffer (Beyotime Biotechnology, P0013), the pellet was eluted with 1x loading buffer and then boiled for 10 min at 100°C. After the samples was cooled, supernatants were loaded on the SDS-PAGE gel and analyzed by western blotting. For IP-MS analysis, the mass spectrometry was performed and analyzed by Shanghai Applied Protein Technology Co. Ltd in China.

## Transfection

ATG7, SQSTM1 and NLRP3 siRNAs, and control siRNA were designed by Guangzhou RiboBio Company. We used riboFECTTM CP Transfection Kit (166T) following the manufacturer's instructions (RiboBio, C10511-05) to transfect THP-1 cells with siRNAs. The following plasmids were purchased from Genecopoeia Company: CMV-SQSTM1-eGFP, CMV-SQSTM1<sup>D335,336,337A</sup>-eGFP and control plasmid. Plasmids were checked by DNA sequencing. The cells were transfected with plasmids (100 nM) using Lipofectamine 3000 (Life Technologies, L3000015) following the manufacturer's instruction.

The THP-1 cells were infected by dual-tagged LC3 (mRFP-GFP-LC3) lentivirus (Hanbio Biotechnology) for autophagy flux analysis. In brief, the cells were incubated by 40 MOI lentivirus for 24 h and treated with LPS for 12 h. Then, the cells were treated by ATP for 20 min with or without LIPUS treatment. After 1 h, the cells harvested and stained by DAPI (1:1000; Sigma-Aldrich, D8417) for 10 min. RFP and GFP LC3B<sup>+</sup> puncta/cell were counted, and forty cells were counted in each group.

## Transmission electron microscopy

Briefly, THP-1 cells were fixed in 2% glutaraldehyde overnight at 4°C. Sections were cut at 60–80 nm and then mounted on copper grids. Sections were impregnated in 2% uranyl acetate and lead citrate. Autophagic vacuoles were detected with an electron microscope (JEM-1011, JEOL/MegaView III, Olympus, Tokyo, Japan).

## Animal experiments

All experiments were performed by the Institutional Animal Care and Use Committee of Daping Hospital. For the model of osteoarthritis, as previously described, DMM surgery was performed on the right knee joints of 10–12 week old C57BL/6 mice [68]. One day after surgery, we anesthetized the mice and smear some coping gel on the right knee. Then, we set the LIPUS device on the injured knee for 20 min/d, 6 d/week. We affixed the LIPUS device to the control mice without electricity at the same time. Two weeks later, the mice were sacrificed by euthanasia and the whole joints were separated. The joint tissues were fixed in 4% paraformaldehyde and decalcified for about 14 d in 15% EDTA. The decalcified joint tissues were dehydrated in 30% sucrose-PBS. The skeleton tissues were then embedded with frozen section medium (Thermo Scientific, 6502) for frozen sections.

For the air pouch model, the protocol was adapted from the previous literature [69]. Briefly, 10–12 weeks old C57BL/6 mice were anesthetized with pentobarbital sodium (50 mg/kg body weight) and 5 mL of sterile air were injected into the skin on the dorsum of mice on day 1. Three days later, 3 mL of sterile air were reinjected into the same cavity. On day 7, inflammation was produced by subcutaneous injection of 1  $\mu$ g of LPS, which was dissolved in 1 mL sterile 0.9% saline solution. For control group, only sterile 0.9% saline solution contain PBS was injected into air pouch. Sixty minutes later, mice were anesthetized and the LIPUS device was used to treat the skin on the dorsum that was coated by coping gel. Twenty-three hours later, mice were treated with LIPUS again. The LIPUS device was activated for 20 min per time. All mice were sacrificed 1 h after the last LIPUS treatment. All mice were allowed to move freely and take water and food *ad libitum* after every treatment. 1 mL sterile 0.9% saline solution was used to lavage the exudates before the sacrifice of mice. The supernatants of exudates were measured for IL1B levels using mouse IL1B ELISA Kit. For tissue histology, the skin tissues were fixed in 4% PFA overnight, and dehydrated by 30% sucrose-PBS at 4°C until the tissues are settled. The tissues were embedded with frozen section medium and sectioned at a thickness of 10  $\mu$ m. Frozen sections were brought to 37°C for

0.5 h and stained with hematoxylin for 3 min. Subsequently the sections were washed with water and then incubated with acid alcohol (0.5% HCl in 70% ethanol) for 20 s. Sections were then washed again and stained with eosin for 20 s.

### Immunofluorescence staining

The cells were seeded into glass-bottom dishes and cultured. After treatment, the cells were washed with PBS and fixed in 4% PFA for 10 min on ice. Then cells were incubated with blocking buffer (Beyotime Biotechnology, P0260) at 37°C for 30 min. After blocking, the cells were incubated with primary antibodies, ADGRE1/F4/80 (Abcam, ab6640), PYCARD/ASC (Cell Signaling Technology, D2W8U), IL1B, LC3B, PKM and SQSTM1 at 1:100 ratio overnight at 4°C. The cells were washed 3 times with PBS and incubated with secondary antibodies. Thereafter, the cells were stained by DAPI for 10 min and confocal laser scanning microscope (Leica TCS SP5 X, Germany) were used to observe the fluorescence change. The frozen tissue sections were handled with the similar protocol.

### Gait analysis

We measured mouse gait before DMM surgery and 1, 7 and 14 d after surgery using the Catwalk apparatus (Noldus, Netherlands). Every mouse was trained at least 2 d until the mouse passed the runway at a relative constant speed without hesitate before the first measurement. During the test, the paw prints of mice were reflected by LED light which was emitted from the glass plate and then detected by the video camera. For gait analysis, at least three eligible step cycles were measured for each mouse at the same time point. The gait data were collected by Catwalk software v10.6 (Noldus). According to the reference manual of Catwalk software, we analyzed the Duty Cycle (%) in each group, and the computational formula was as follows: Duty Cycle = Stand/(Stand + Swing) × 100%.

### Statistical analyses

Data were analyzed using GraphPad Prism version 7.0. All results are revealed as means ± SEM of three independent experiments at least. Statistical significances were calculated with Student's t-test for comparisons between 2 groups and ANOVA for multiple group comparisons as showed in figure legends. P values were considered significant at \*P < 0.05, \*\*P < 0.01, \*\*\*P < 0.001 and \*\*\*\*p < 0.0001.

### Disclosure statement

No potential conflict of interest was reported by the authors.

### Funding

This work was supported by (1) Special Funds for Major State Basic Research Program of China (973 program) (No. 2014CB942900); (2) National Natural Science Foundation of China (No. 81530071, 81871817).

## References

- Wang X, Hunter DJ, Jin X, et al. The importance of synovial inflammation in osteoarthritis: current evidence from imaging assessments and clinical trials. *Osteoarthritis Cartilage*. 2017;26:165–174.
- Roemer FW, Kassim Javid M, Guermazi A, et al. Anatomical distribution of synovitis in knee osteoarthritis and its association with joint effusion assessed on non-enhanced and contrast-enhanced MRI. *Osteoarthritis Cartilage*. 2010;18:1269–1274.
- Sellam J, Berenbaum F. The role of synovitis in pathophysiology and clinical symptoms of osteoarthritis. *Nat Rev Rheumatol*. 2010;6:625–635.
- Kapoor M, Martel-Pelletier J, Lajeunesse D, et al. Role of proinflammatory cytokines in the pathophysiology of osteoarthritis. *Nat Rev Rheumatol*. 2011;7(1):33–42.
- Mathiessen A, Conaghan PG. Synovitis in osteoarthritis: current understanding with therapeutic implications. *Arthritis Res Ther*. 2017;19:18.
- Kraus VB, Mcdaniel G, Huebner JL, et al. Direct in vivo evidence of activated macrophages in human osteoarthritis. *Osteoarthritis Cartilage*. 2016;24:1613–1621.
- Onuora S. Osteoarthritis: molecular imaging detects activated macrophages. *Nat Rev Rheumatol*. 2016;12:313.
- Piscaer TM, Muller C, Mindt TL, et al. Imaging of activated macrophages in experimental osteoarthritis using folate-targeted animal single-photon-emission computed tomography/computed tomography. *Arthritis Rheum*. 2011;63:1898–1907.
- Blom AB, van Lent PL, Holthuysen AE, et al. Synovial lining macrophages mediate osteophyte formation during experimental osteoarthritis. *Osteoarthritis Cartilage*. 2004;12:627–635.
- Hikiji H, Takato T, Shimizu T, et al. The roles of prostanoids, leukotrienes, and platelet-activating factor in bone metabolism and disease. *Prog Lipid Res*. 2008;47:107–126.
- Zhang H, Lin C, Zeng C, et al. Synovial macrophage M1 polarisation exacerbates experimental osteoarthritis partially through R-spondin-2. *Ann Rheum Dis*. 2018;77:1524–1534.
- Bondeson J, Blom AB, Wainwright S, et al. The role of synovial macrophages and macrophage-produced mediators in driving inflammatory and destructive responses in osteoarthritis. *Arthritis Rheum*. 2010;62:647–657.
- Busse JW, Bhandari M, Kulkarni AV, et al. The effect of low-intensity pulsed ultrasound therapy on time to fracture healing: a meta-analysis. *CMAJ*. 2002 19;166:437–441.
- Jia L, Wang Y, Chen J, et al. Efficacy of focused low-intensity pulsed ultrasound therapy for the management of knee osteoarthritis: a randomized, double blind, placebo-controlled trial. *Sci Rep*. 2016;6:35453.
- Rutjes AW, Nuesch E, Sterchi R, et al. Therapeutic ultrasound for osteoarthritis of the knee or hip. *Cochrane Database Syst Rev*. 2010;20: Cd003132.
- Da Silva Junior EM, Mesquita-Ferrari RA, Franca CM, et al. Modulating effect of low intensity pulsed ultrasound on the phenotype of inflammatory cells. *Biomed Pharmacother*. 2017;96:1147–1153.
- Chen SF, Su WS, Wu CH, et al. Transcranial ultrasound stimulation improves long-term functional outcomes and protects against brain damage in traumatic brain injury. *Mol Neurobiol*. 2018;55:7079–7089.
- Itaya N, Yabe Y, Hagiwara Y, et al. Effects of low-intensity pulsed ultrasound for preventing joint stiffness in immobilized knee model in rats. *Ultrasound Med Biol*. 2018;44:1244–1256.
- Lin G, Reed-Maldonado AB, Lin M, et al. Effects and mechanisms of low-intensity pulsed ultrasound for chronic prostatitis and chronic pelvic pain syndrome. *Int J Mol Sci*. 2016;17:E1057.
- Nakao J, Fujii Y, Kusuyama J, et al. Low-intensity pulsed ultrasound (LIPUS) inhibits LPS-induced inflammatory responses of osteoblasts through TLR4–myD88 dissociation. *Bone*. 2014;58:17–25.
- Nagao M, Tanabe N, Manaka S, et al. LIPUS suppressed LPS-induced IL-1α through the inhibition of NF-κB nuclear translocation via AT1-PLCβ pathway in MC3T3-E1. *J Cell Physiol*. 2017;232:3337–3346.

- [22] Zhang X, Hu B, Sun J, et al. Inhibitory effect of low-intensity pulsed ultrasound on the expression of lipopolysaccharide-induced inflammatory factors in U937 cells. *J Ultrasound Med.* 2017;36:2419–2429.
- [23] Gabriel AF, Marcus MA, Honig WM, et al. The CatWalk method: a detailed analysis of behavioral changes after acute inflammatory pain in the rat. *J Neurosci Methods.* 2007;163:9–16.
- [24] Syed R. Evaluating the limping child: a rheumatology perspective. *Mo Med.* 2016;113:131–135.
- [25] Jackson MT, Moradi B, Zaki S, et al. Depletion of protease-activated receptor 2 but not protease-activated receptor 1 may confer protection against osteoarthritis in mice through extracartilaginous mechanisms. *Arthritis Rheumatol.* 2014;66:3337–3348.
- [26] Kadl A, Galkina E, Leitinger N. Induction of CCR2-dependent macrophage accumulation by oxidized phospholipids in the air-pouch model of inflammation. *Arthritis Rheum.* 2009;60:1362–1371.
- [27] Jin C, Frayssinet P, Pelker R, et al. NLRP3 inflammasome plays a critical role in the pathogenesis of hydroxyapatite-associated arthropathy. *Proc Natl Acad Sci U S A.* 2011;108:14867–14872.
- [28] Venegas C, Kumar S, Franklin BS, et al. Microglia-derived ASC specks cross-seed amyloid-beta in Alzheimer's disease. *Nature.* 2017;552:355–361.
- [29] He Y, Hara H, Nunez G. Mechanism and regulation of NLRP3 inflammasome activation. *Trends Biochem Sci.* 2016;41:1012–1021.
- [30] Mariathasan S, Weiss DS, Newton K, et al. Cryopyrin activates the inflammasome in response to toxins and ATP. *Nature.* 2006;440:228–232.
- [31] Coll RC, Robertson AA, Chae JJ, et al. A small-molecule inhibitor of the NLRP3 inflammasome for the treatment of inflammatory diseases. *Nat Med.* 2015;21:248–255.
- [32] Keller M, Rüegg A, Werner S, et al. Active caspase-1 is a regulator of unconventional protein secretion. *Cell.* 2008;132:818–831.
- [33] Shi CS, Shenderov K, Huang NN, et al. Activation of autophagy by inflammatory signals limits IL-1beta production by targeting ubiquitinated inflammasomes for destruction. *Nat Immunol.* 2012;13:255–263.
- [34] Takahama M, Akira S, Saitoh T. Autophagy limits activation of the inflammasomes. *Immunol Rev.* 2018;281:62–73.
- [35] Saitoh T, Fujita N, Jang MH, et al. Loss of the autophagy protein Atg16L1 enhances endotoxin-induced IL-1beta production. *Nature.* 2008;456:264–268.
- [36] Klionsky D, Klionsky D, Abdelmohsen K, et al. Guidelines for the use and interpretation of assays for monitoring autophagy (3rd edition) - eScholarship. *Autophagy.* 2016;12:1–222.
- [37] Yamamoto A, Tagawa Y, Yoshimori T, et al. Bafilomycin A1 prevents maturation of autophagic vacuoles by inhibiting fusion between autophagosomes and lysosomes in rat hepatoma cell line, H-4-II-E cells. *Cell Struct Funct.* 1998;23:33–42.
- [38] Huang R, Xu Y, Wan W, et al. Deacetylation of nuclear LC3 drives autophagy initiation under starvation. *Mol Cell.* 2015;57:456–466.
- [39] Kimura S, Noda T, Yoshimori T. Dissection of the autophagosome maturation process by a novel reporter protein, tandem fluorescent-tagged LC3. *Autophagy.* 2007;3:452–460.
- [40] Mizushima N, Yoshimori T, Levine B. Methods in mammalian autophagy research. *Cell.* 2010;140:313–326.
- [41] Bjørkøy G, Lamark T, Brech A, et al. p62/SQSTM1 forms protein aggregates degraded by autophagy and has a protective effect on huntingtin-induced cell death. *J Cell Biol.* 2005;171(4):603–614.
- [42] Choe JY, Jung HY, Park KY, et al. Enhanced p62 expression through impaired proteasomal degradation is involved in caspase-1 activation in monosodium urate crystal-induced interleukin-1b expression. *Rheumatology (Oxford).* 2014;53:1043–1053.
- [43] Ohtsuka S, Ishii Y, Matsuyama M, et al. SQSTM1/p62/A170 regulates the severity of Legionella pneumophila pneumonia by modulating inflammasome activity. *Eur J Immunol.* 2014;44:1084–1092.
- [44] Ichimura Y, Kumanomidou T, Sou YS, et al. Structural basis for sorting mechanism of p62 in selective autophagy. *J Biol Chem.* 2008;283(33):22847–22857.
- [45] Matsumoto G, Wada K, Okuno M, et al. Serine 403 phosphorylation of p62/SQSTM1 regulates selective autophagic clearance of ubiquitinated proteins. *Mol Cell.* 2011;44:279–289.
- [46] Palsson-McDermott EM, O'Neill LA. The Warburg effect then and now: from cancer to inflammatory diseases. *Bioessays.* 2013;35:965–973.
- [47] Xie M, Yu Y, Kang R, et al. PKM2-dependent glycolysis promotes NLRP3 and AIM2 inflammasome activation. *Nat Commun.* 2016;7:13280.
- [48] O'Neill TW, Parkes MJ, Maricar N, et al. Synovial tissue volume: a treatment target in knee osteoarthritis (OA). *Ann Rheum Dis.* 2016;75:84–90.
- [49] Evans CH, Kraus VB, Setton LA. Progress in intra-articular therapy. *Nat Rev Rheumatol.* 2014;10:11–22.
- [50] Cotero V, Fan Y, Tsaava T, et al. Noninvasive sub-organ ultrasound stimulation for targeted neuromodulation. *Nat Commun.* 2019;10:952.
- [51] Zachs DP, Offutt SJ, Graham RS, et al. Noninvasive ultrasound stimulation of the spleen to treat inflammatory arthritis. *Nat Commun.* 2019;10:951.
- [52] Sachs D, Cunha FQ, Poole S, et al. Tumour necrosis factor-alpha, interleukin-1beta and interleukin-8 induce persistent mechanical nociceptor hypersensitivity. *Pain.* 2002;96:89–97.
- [53] Samad TA, Moore KA, Sapirstein A, et al. Interleukin-1beta-mediated induction of Cox-2 in the CNS contributes to inflammatory pain hypersensitivity. *Nature.* 2001;410:471–475.
- [54] Kraus VB, Birmingham J, Stabler TV, et al. Effects of intra-articular IL1-Ra for acute anterior cruciate ligament knee injury: a randomized controlled pilot trial (NCT00332254). *Osteoarthritis Cartilage.* 2012;20:271–278.
- [55] Hayward JA, Mathur A, Ngo C, et al. Cytosolic recognition of microbes and pathogens: inflammasomes in action. *Microbiol Mol Biol Rev.* 2018;82:e00015–18.
- [56] McAllister MJ, Chemaly M, Eakin AJ, et al. NLRP3 as a potentially novel biomarker for the management of osteoarthritis. *Osteoarthritis Cartilage.* 2018;26:612–619.
- [57] Evavold CL, Ruan J, Tan Y, et al. The pore-forming protein gasdermin D regulates interleukin-1 secretion from living macrophages. *Immunity.* 2018;48:35–44.
- [58] Watanabe Y, Tanaka M. p62/SQSTM1 in autophagic clearance of a non-ubiquitylated substrate. *J Cell Sci.* 2011;124:2692–2701.
- [59] Pankiv S, Clausen TH, Lamark T, et al. p62/SQSTM1 binds directly to Atg8/LC3 to facilitate degradation of ubiquitinated protein aggregates by autophagy. *J Biol Chem.* 2007;282:24131–24145.
- [60] Spalinger MR, Lang S, Gottier C, et al. PTPN22 regulates NLRP3-mediated IL1B secretion in an autophagy-dependent manner. *Autophagy.* 2017;13:1590–1601.
- [61] Zhong Z, Umemura A, Sanchez-Lopez E, et al. NF-kappaB restricts inflammasome activation via elimination of damaged mitochondria. *Cell.* 2016;164:896–910.
- [62] Lee J, Kim HR, Quinley C, et al. Autophagy suppresses interleukin-1beta (IL-1beta) signaling by activation of p62 degradation via lysosomal and proteasomal pathways. *J Biol Chem.* 2012;287:4033–4040.
- [63] Viana R, Lujan P, Sanz P. The laforin/malin E3-ubiquitin ligase complex ubiquitinates pyruvate kinase M1/M2. *BMC Biochem.* 2015;16:24.
- [64] Liu K, Li F, Han H, et al. Parkin regulates the activity of pyruvate kinase M2. *J Biol Chem.* 2016;291:10307–10317.



- [65] Shang Y, He J, Wang Y, et al. CHIP/Stub1 regulates the Warburg effect by promoting degradation of PKM2 in ovarian carcinoma. *Oncogene*. 2017;36:4191–4200.
- [66] Seibenhener ML, Babu JR, Geetha T, et al. Sequestosome 1/p62 is a polyubiquitin chain binding protein involved in ubiquitin proteasome degradation. *Mol Cell Biol*. 2004;24: 8055–8068.
- [67] Palsson-McDermott EM, Curtis AM, Goel G, et al. Pyruvate kinase M2 regulates Hif-1alpha activity and IL-1beta induction and is a critical determinant of the Warburg effect in LPS-activated macrophages. *Cell Metab*. 2015 Feb 3;21:65–80.
- [68] Glasson SS, Blanchet TJ, Morris EA. The surgical destabilization of the medial meniscus (DMM) model of osteoarthritis in the 129/SvEv mouse. *Osteoarthritis Cartilage*. 2007;15:1061–1069.
- [69] Liu-Bryan R, Scott P, Sydlaske A, et al. Innate immunity conferred by Toll-like receptors 2 and 4 and myeloid differentiation factor 88 expression is pivotal to monosodium urate monohydrate crystal-induced inflammation. *Arthritis Rheum*. 2005; 52:2936–2946.